Chapter 2

Diagnosing Tropical Cyclone Rapid Intensification Through Rotated Principal Component Analysis of Synoptic-Scale Diagnostic Fields

Alexandria Grimes and Andrew E. Mercer

Additional information is available at the end of the chapter

http://dx.doi.org/10.5772/63988

Abstract

Forecasts of rapid intensification (RI) within tropical cyclones continue to be a major challenge, primarily due to difficulty in determining the processes that distinguish RI and non-RI storms. In this study, the aim was to identify the most important RI/non-RI discriminatory variables in the North Atlantic basin, not only by level, but also spatial location relative to the tropical cyclone center. These important variables, identified using rotated principal component analysis on one-dimensional and three-dimensional GEFS reforecast base-state variables from 1985 to 2009, led to the identification of diagnostic fields with the largest variability between RI and non-RI events. Hierarchical clustering techniques performed on rotated PC loadings provided map types of RI and non-RI cyclones. Analysis of these composite map types, as well as composite derived fields including divergence, relative vorticity, equivalent potential temperature, static stability, and vertical shear, revealed interesting distinguishing characteristics between RI and non-RI events. Results suggested that vorticity in the mid-levels, divergence in the upper-levels, equivalent potential temperature, and specific humidity play critical roles in successfully discriminating between RI and non-RI storms. These findings give key insights to which variables should be used in developing a prognostic classification scheme to assist with operational forecasts of tropical cyclone RI.

Keywords: tropical cyclone, rapid intensification, principal component analysis, cluster analysis, kinematic and thermodynamic tropical meteorology

1. Introduction

Modern statistical and dynamic forecast models continue to demonstrate low forecast skill in identifying the onset of rapid intensification (hereafter known as RI) within tropical cyclones (hereafter known as TCs). Even though storms which rapidly intensify can cost governments billions of dollars in damage upon landfall (e.g. by destroying property through flooding–as with Katrina in 2005) and RI forecasting is considered one of the top priorities for the National Hurricane Center [1], little advancement has been made in improvement of probabilistic tropical cyclone RI forecasting. While previous studies have examined the intensification patterns between RI and non-RI TCs [2, 3], the technological impairments, coupled with the complexity of these systems, have left gaps in understanding the large-scale structures associated with RI storms [1–4]. These gaps result in poor statistical forecast model accuracy, which requires prior knowledge of relevant RI variables. While recent research shows modest improvements in RI forecasts, and global models have steadily improved in their ability to predict the large-scale environmental conditions of TCs [3], forecast skill scores still remain inadequate.

Current statistical forecast models blend both thermodynamic and kinematic variables in attempts to increase the skill, emphasizing meteorological processes deemed more crucial to RI prediction [1, 4–6]. Improvements to the Statistical Hurricane Intensity Prediction Scheme Rapid Intensification Index (SHIPS-RII) continue to be added regularly since the original implementation by the National Hurricane Center (NHC) in 2004 for the North Atlantic [1]. The latest enhanced SHIPS-RII consists of 10 predictors, including previous 12-hour intensity change, vertical shear, divergence at 200 hPa, total precipitable water, GOES-IR imagery, potential intensity, oceanic heat content, max sustained wind, and an inner-core dry air predictor [1]. Despite the addition of new predictors, Brier skill scores (BSS) relative to climatology for Atlantic RI forecasts remain below 20% [1]. Additionally, verification of all operational consensus intensity forecast models for the NHC, including their official intensity forecast, showed only limited improvement as Peirce skill scores remained below 0.2 [1]. Other studies have included predictors that resolve the inner-core environment more effectively, utilizing microwave passive imagery predictors in a probabilistic logistic regression (LR) model. Despite this effort, BSS values only improved to roughly 22% with either simulated real-time LR models or LR models utilizing reanalysis data [4]. Additionally, using a baseline peak wind speed of 25 knot intensity (at all RI thresholds) severely reduces skill to below 15% when compared to a probabilistic LR model utilizing current SHIPS parameters previously developed in [7].

In order to improve statistical model prediction of the onset of TC RI, the ability to identify distinguishing meteorological characteristics of the storm structure between RI and non-RI TCs with 24 hours lead time is crucial. While research of this nature is not new [2, 3], the approaches have differed (e.g. data selection, data reduction, meteorological variables chosen, compositing approaches). For example, Kaplan and DeMaria [2] and Kaplan et al. [8] noted that RI was more likely to occur for TCs that were situated over regions of higher than average sea surface temperature (SST), strong upper-level divergence, large low- to mid-tropospheric

moisture, and weaker than average vertical wind shear [2, 8]. Other research (see [3]) also observed that RI events occurred in environments with weaker deep-layer shear (as was found in [2, 8]) and greater conditional instability in the Atlantic basin than non-RI events. This research also noted that TCs moving over a warm ocean anomaly were found to be equally likely to intensify slowly or rapidly given other assumptions are met [3], a result in contrast with the work shown in [2, 8]. While recent research suggests environmental, internal dynamic processes, and oceanic conditions [2, 3, 8] all play a role in RI, research performed in [3] concluded RI is mostly controlled by internal dynamical processes, provided a pre-existing favorable environment exists. Research performed in [4] reiterated this sentiment suggesting Atlantic basin forecasts benefit more from the inclusion of storm structure information (more than the Pacific basins), which has yet to be explained.

In an effort to continue improving the understanding of the internal dynamics of TCs undergoing RI, the current study sought to identify important diagnostic variables in the North Atlantic basin, looking not only at which levels, but also at which spatial points in proximity to the cyclone are distinguishable between the two types of systems. The primary research question being considered is: What meteorological parameters discriminate RI from non-RI storms most effectively, and what spatial location in the TC domain provide the largest differences in these fields? These findings give key insights to which variables should be used in future development of a prognostic artificial intelligence classification scheme to assist with operational forecasts of RI. Section 2 provides a description of the data and methodology, while Section 3 presents the results of the work and Section 4 provides a discussion and conclusions.

2. Data and methodology

2.1. Dataset description

While the NHC defines RI as an increase in wind of 30 knots (kt) in 24 hours, several RI definitions are usually considered during the research phase of model development [1, 4]. This study examined three separate definitions of RI (following [1]), including the operational definition of a 30kt increase of wind speed in 24 hours and two experimental definitions of 25kt and 40kt increases. All Atlantic tropical and subtropical systems, from 1985–2009 from the NHC Atlantic best track data (HURDAT–[9]) were considered. For the three different RI definitions, the full database of 298 TC events were divided into RI and non-RI groups, yielding 152 RI and 146 non-RI cases with the 25kt definition, 119 RI and 179 non-RI for the 30kt definition, and 46 RI and 252 non-RI for the 40kt definition (**Figure 1** breaks these down by Saffir-Simpson scale category). Since a forecast proxy was desired, base-state meteorological fields from the National Centers for Environmental Prediction (NCEP) Global Ensemble Forecast System (GEFS–[10]) reforecast database were retained 24 hours prior to the period of greatest intensification for all storms (RI and non-RI). GEFS reforecast data are provided at a 1° resolution at 3-hour forecast intervals from 0 to 72-hours. Three-dimensional base-state meteorological fields at eight vertical levels (1000–100 hPa) were utilized, including: geopotential height, temperature, u and v wind components, and specific humidity. Additionally,

single-layer variables were considered, including mean sea level pressure (MSLP), skin temperature (a proxy for SST), latent heat flux, sensible heat flux, convective available potential energy (CAPE), convective inhibition (CIN), and vertical velocity at 850 hPa were evaluated.

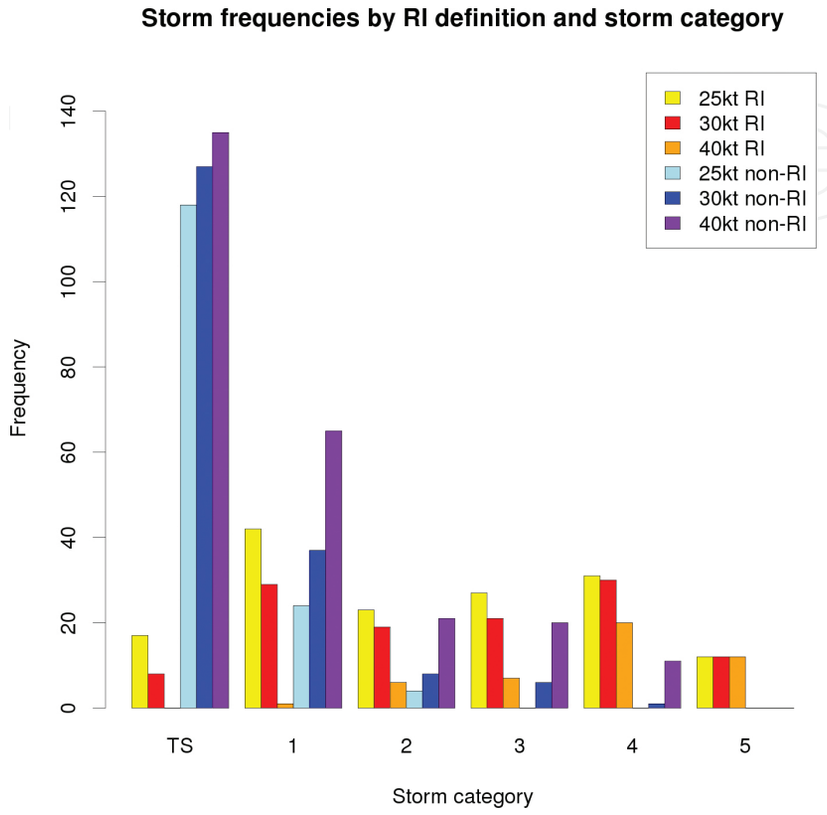

Figure 1. Distribution of category per TC event type per RI definition using 25kt/24-hours, 30kt/24-hours, and 40kt/24-hours definitions.

As a primary goal was to diagnose RI using TC structure relative to the storm center, storm-centric GEFS reforecast domains for each cyclone were obtained. Storm centers were identified by determining the local minimum in GEFS MSLP nearest the NHC-defined TC center, 24-hours prior to the timestep associated with the greatest intensification. Each variable was retained on a 15° × 11° latitude/longitude grid centered on this domain. In the event multiple occurrences of peak intensification occurred for an individual TC (which occurred 28 times when using 25kt/24-hours, 13 times for 30kt/24-hours, and once for 40kt/24-hours), the first was chosen. Thus, the results presented herein deal with the first instance of peak intensification regardless of the frequency of peak intensification for a given TC.

2.2. RPCA

As the primary goal of this research was the identification of variables and spatial locations most favorable for distinguishing RI and non-RI storms, discriminatory statistical methods were needed. One method, rotated principal component analysis (RPCA), has been shown to be useful in discriminating meteorological environments of different types [11–14]. These

studies also used permutation testing to evaluate magnitude differences in diagnostic variables for each environment. Both of these techniques were utilized in the current study so that both spatial configuration and magnitude difference could be assessed.

2.2.1. S-mode RPCA

The first approach to RPCA, S-mode analysis [13], provided a diagnosis of the spatial relationship among gridpoints for all cases. For S-mode, the similarity matrix is computed on the individual spatial locations and is eigenanalyzed to identify particular locations that group together. The S-mode rotated principal component (RPC) loadings are maps that demonstrate these spatial relationships (known as modes of variability), with the RPC scores revealing the similarity between the individual cases and the resulting S-mode loading maps. To reduce the dimensions of the eigenvector matrix, truncation of RPCs was completed by evaluating a scree plot, as well as using a congruence test. A congruence test is a way to measure pattern and magnitude similarity of a dataset, corresponding to the cosine of the angular separation between the loadings, by maximizing the dissimilarity of the two loading patterns [15]. The congruence coefficient presenting a strong relationship for any absolute value greater than 0.81 was marked as the truncation point. RI and non-RI datasets (consisting only of base-state variables for all 298 cases) were combined, where the analysis of both RI and non-RI event

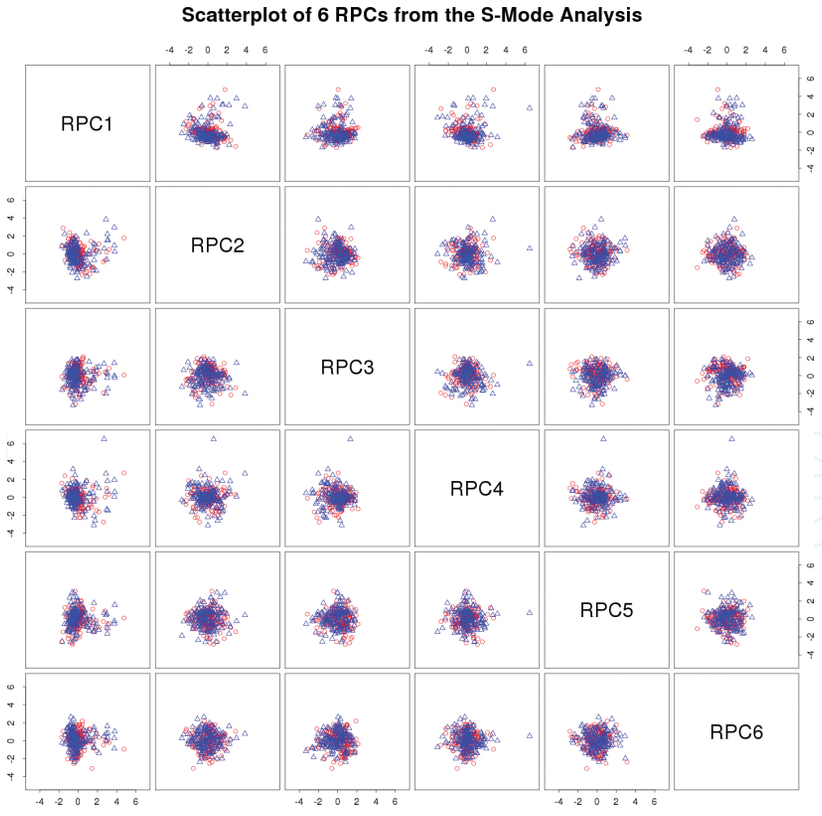

Figure 2. Pairwise scatterplots of all six PC score vectors. RI PC scores are redpoints, while non-RI points are blue. The significant overlap among the groups demonstrates the challenges in linearly separating these types of TCs.

deviations and the loading patterns provided information on how the systems are grouping together (e.g. cooler SSTs versus warmer, upper level trough/ridge patterns, and influence of land at the surface 24-hours prior). To demonstrate the lack of linear separability in the resulting RPCs, a pairwise scatterplot of all six PC score vectors was formulated (**Figure 2**). There is significant overlap among the RI and non-RI PC scores, rendering separation via classification very difficult, motivating the need to consider additional analysis techniques.

		Variance explained (%)					
		25kt/24-hours		30kt/24-hours		40kt/24-hours	
	S-mode	T-mode		T-mode		T-mode	
RPCs	Combined	RI	non-RI	RI	non-RI	RI	non-RI
1	24	18	13	14	12	16	11
2	12	11	12.8	11	13	11	14
3	7.4	7.6	4.8	7.7	5.0	7.3	6.3
4	3.6	6.6	7.7	7.2	7.8	7.0	8.4
5	4.5	4.7	4.7	4.9	5.8	5.4	4.8
6	3.3	—	4.5	—	—	—	—

Table 1. Rotated principal components variance explained for S-mode, as well as T-mode, for each event type and each RI definition. Dashes simply mean that this number of RPCs was not retained based on the previously described testing methodologies.

2.2.2. T-mode RPCA

While S-mode helped reveal the difficulties in identifying relevant RI/non-RI distinguishing characteristics, the results did not provide the necessary discrimination capability of interest in this work. Recent work has shown the value of composite analysis with T-mode RPCA in identifying discriminating characteristics for different meteorological event types [11, 12]. Following the methodology of [11, 12], a T-mode varimax-rotated RPCA [11, 16], conducted simultaneously on all GEFS reforecast fields, was completed on all RI events and all non-RI events separately. T-mode contrasts S-mode in that in T-mode, the relationships between events, as opposed to spatial locations, are of interest, and thus the correlation matrix is computed on the event dimension of the data. Following methods established in [11, 12], the resulting uncorrelated eigenvector matrix and associated eigenvalues reduced to a subset of RPCs for each event type and each RI definition (**Table 1**). Similar to the S-mode RPCA approach, the truncation point was determined through utilization of a scree plot and the congruence test. The resulting RPC loadings maintain the same dimension as the event dimension, so events were clustered by RPC loading magnitude using hierarchical clustering with Ward's minimum variance method [16]. To assess cluster quality, a cluster verification statistic (silhouette coefficient [17]) was found that includes two components:

1. a measure of intra-cluster spread (cluster cohesion–should be small) and

2. a measure of inter-cluster spread (cluster separation–should be large) [11].

In this study, the mean of the silhouette coefficient values for all events considered in the cluster analysis was retained as a measure of cluster analysis performance. With the silhouette coefficient, values approaching 1 suggest a minimization of cluster cohesion and a maximization of cluster separation. Negative values suggest a particular event was misclustered. The cluster analysis revealed six clusters each for RI and non-RI storm types using the 25kt/24-hours definition, seven non-RI and six RI using the 30kt/24-hours definition, and seven non-RI and five RI using the 40kt/24-hours definition (**Table 2** provides the number of events per cluster, as well as silhouette coefficient values). Events within each cluster were averaged together, yielding map types that retained unique synoptic-scale structures and provided more detailed map types of RI and non-RI TC environments than simply averaging all events together. The resulting composites allowed for the identification of spatial structure among RI/non-RI events.

	T- mode cluster distribution and Silhouette coefficients (S.C.)		
RI	**25kt/24-hours**	**30kt/24-hours**	**40kt/24-hours**
S.C.	0.24	0.24	0.26
1	22	18	9
2	28	21	**14**
3	18	25	8
4	13	27	9
5	**40**	**28**	6
6	31	—	—
non-RI			
S.C.	0.20	0.21	0.22
1	23	25	31
2	26	21	40
3	**37**	15	**55**
4	16	18	33
5	21	38	24
6	23	**47**	28
7	—	15	41

Table 2. Silhouette coefficients and number of events per cluster through Ward's method on T-mode RPC loadings.

2.3. Permutation testing

While the composites resulting from the RPCA approach are useful for diagnosing spatial characteristics within RI and non-RI environments, magnitude differences are diagnosed more effectively using hypothesis testing. In this study, permutation tests [16] comparing magni-

tudes of diagnostic fields in RI and non-RI storms were utilized at each gridpoint from the study domains, yielding a spatial map of significance values associated with each variable tested. The resulting plots provided specific regions in the study domain where statistically significant magnitude differences between RI and non-RI storms existed for individual GEFS reforecast variables. These results provided insight not only into the scope of these magnitude differences but into the spatial locations of the differences, which complement the RPCA results well.

3. Analysis

Based on previous work done [12], variables selected for evaluation consisted of base-state variables and derived variables as listed in Section 2.1. Through the S-mode technique, only base-state variables were examined; therefore, only notable characterizations are summarized in the text below. The T-mode and cluster analysis technique; however, yielded numerous composite fields for consideration. To minimize this impact, the cluster from each RI group and each RI definition that contained the largest number of events (bolded in **Table 2**) is provided for discussion below.

3.1. RI and non-RI S-mode maps

As stated previously, S-mode analysis of the base-state meteorological fields was conducted first. **Table 1** shows that RPC1 contained the largest variance explained (roughly 24%), and the loading map (**Figure 3**) revealed that areas of higher heights in the northeast quadrant quadrant and over the storm center co-varied with higher MSLP, lower temperatures, lower moisture and latent heat content. A total of 16 events' RPC scores (**Table 3**) exceeded 2 standard deviations above the mean, suggesting strong positive correlation between those events and RPC1. Of these 16 events, six were classified as RI cases with the 25kt/24-hour definition of RI. In fact, the highest positive deviation (approximately 5 standard deviations above the mean) was an RI case, while the second largest positive deviations were a mixture of RI and non-RI events. These results suggest a blend of RI and non-RI events for RPC1. Similarly, RPC2 results (which explained approximately 12% of the variability) revealed lower heights in proximity of the storm center (**Figure 4**) co-varied with lower MSLP, cooler low-level temperatures in the southwest quadrant of the cyclone and overall higher specific humidity and latent heat flux values. Additionally, patterns revealing a wrap-around of moisture over the storm-center were revealed. However, only three of the eight events that exceeded 2 standard deviations from the mean were RI events, again showing the blending of RI and non-RI cases in these results. RPC3 (which explained approximately 7% of the total variance), exhibited higher heights co-located with higher MSLP, temperature, specific humidity, and latent heat flux over the storm center and to the south, but lower heights, temperature, specific humidity, and latent heat flux North of the storm center (**Figure 5**). This RPC profile, along with RPCs 4–6 (not shown), is indicative of baroclinic environmental influence associated with both storm types. These first three RPCs, explaining over half of the variability combined, demonstrated a recurring

http://dx.doi.org/10.5772/63988

problem in the S-mode analysis, namely the inability to separate RI and non-RI events (as was seen in **Figure 2**).

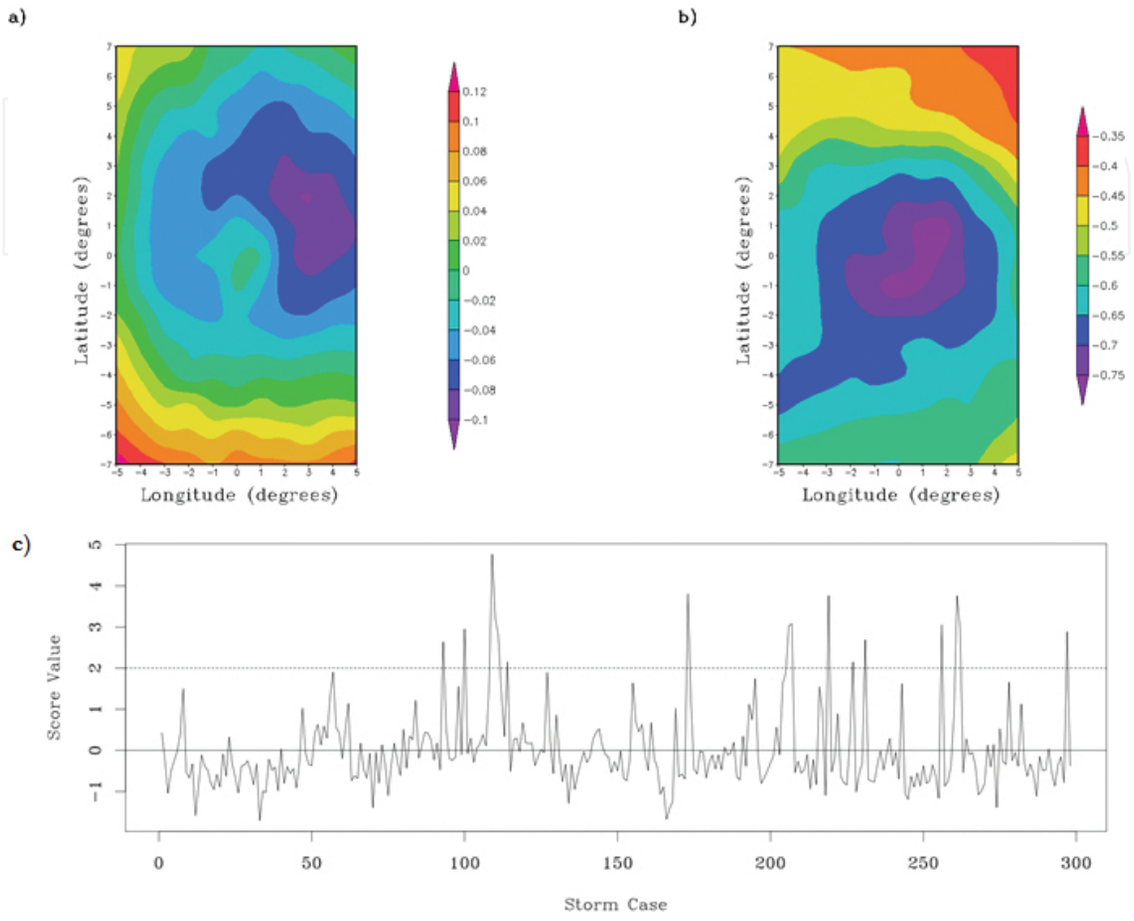

Figure 3. S-mode RPC 1 loading patterns for geopotential height at 850 hPa (panel a) and specific humidity at 850 hPa (panel b) with respect to latitude/longitude relative to the storm center, as well as the associated RPC score time series (panel c). The product of the loading map and its time-series value for a case are in units of standard anomalies.

	S-mode score extremes (±) 2 SDs above mean			
	+2 SD RI	**−2 SD RI**	**+2 SD non-RI**	**−2 SD non-RI**
RPC 1	6	0	10	0
RPC 2	3	4	5	4
RPC 3	1	5	0	8
RPC 4	3	4	4	5
RPC 5	2	7	4	4
RPC 6	1	6	2	2

Table 3. RPC score values exceeding (±) 2 standard deviations above/below the mean.

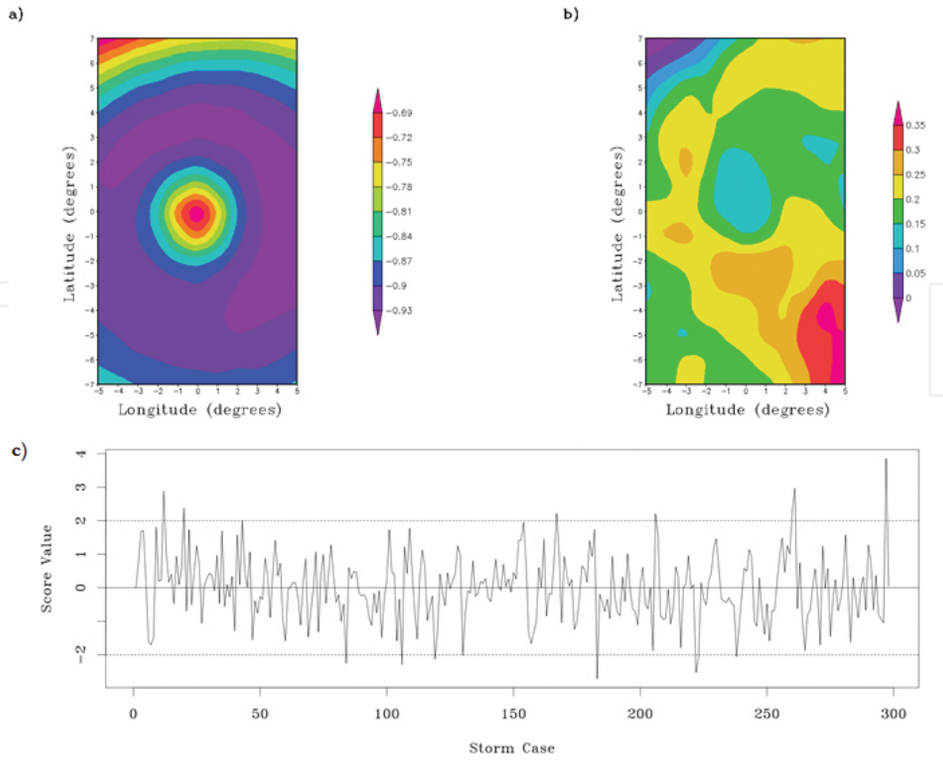

Figure 4. Same as **Figure 3**, but for RPC 2.

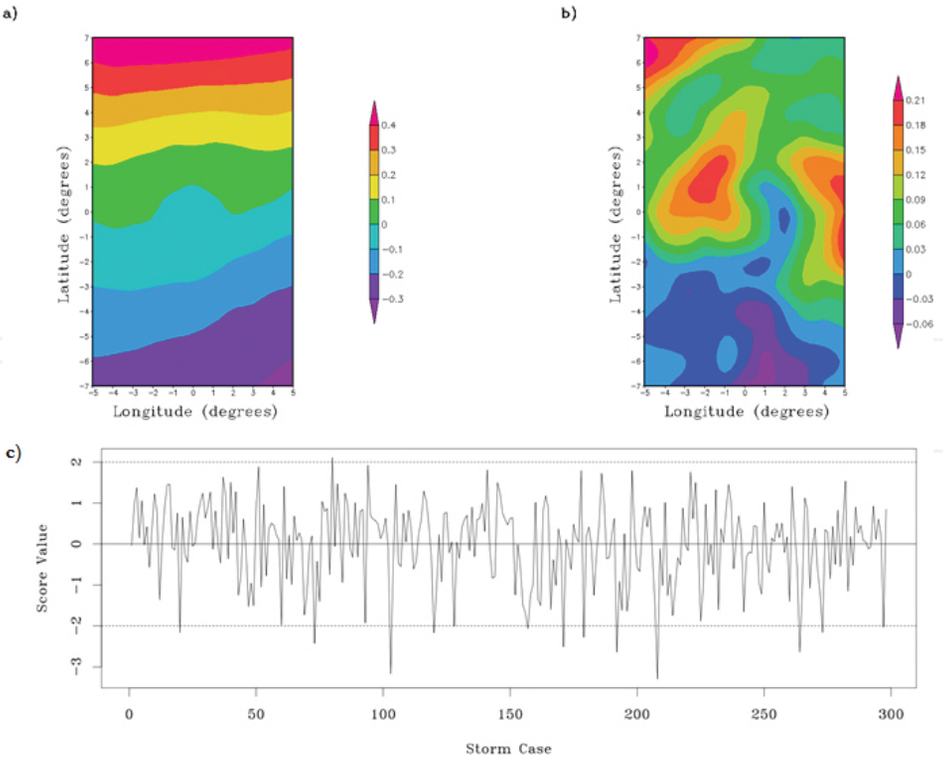

Figure 5. Same as **Figure 3**, but for RPC 3.

Through this analysis, the inherent difficulty of classifying RI and non-RI storms is apparent, as the base-state fields considered seem to be equally present in RI and non-RI events for all RPCs. Despite this, the results suggest some modest classification ability of RI and non-RI events through the temperature and moisture patterns, as well as variables more indicative of environmental interaction (e.g. vorticity and static stability) as the largest influences on TC RI processes.

3.2. RI and non-RI T-mode composites

T-mode composites of the base-state meteorological fields, as well as derived fields including: divergence, relative vorticity, vertical speed and directional wind shears (see [18] for clarification on the difference), equivalent potential temperature, and static stability (as defined in [19]) were formulated next. The analysis below is broken down by variable.

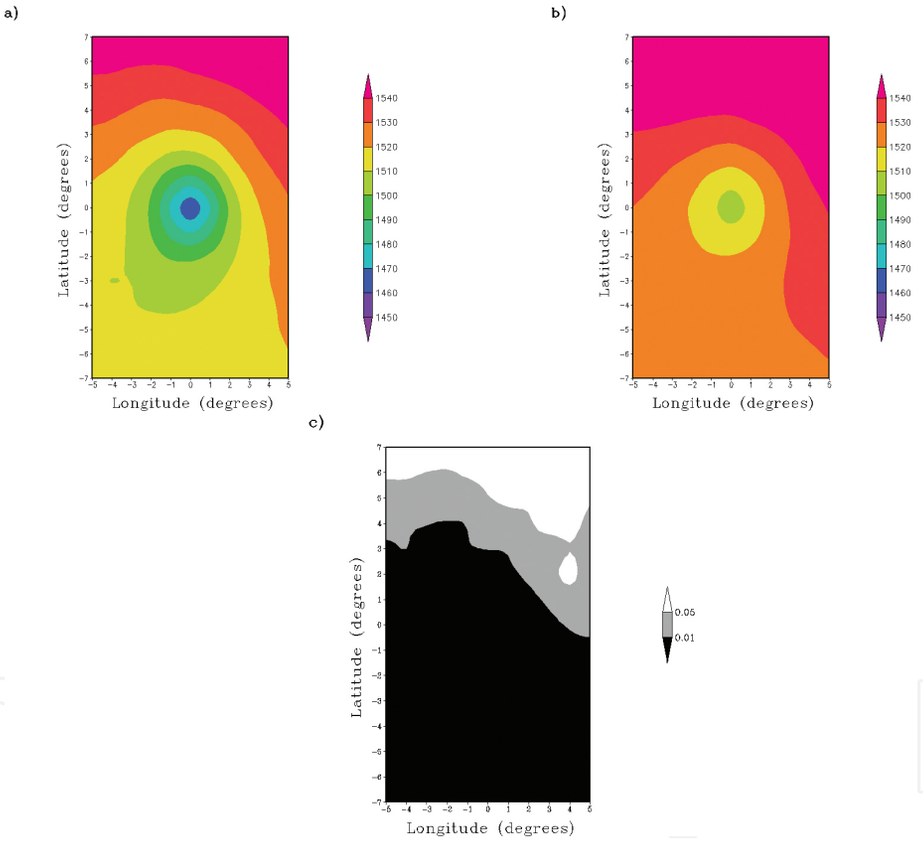

Figure 6. Geopotential height (m), with respect to latitude/longitude relative to the storm center, composites at 850 hPa using 40kt/24-hours definition for cluster 2 RI (panel a) and cluster 3 non-RI (panel b). Permutation tests results (panel c–shaded areas are significant at α=0.05 or less) revealed nearly the entire map as significant in discriminating between RI and non-RI events.

3.2.1. Geopotential height and mean sea level pressure characteristics

The map types for RI and non-RI systems revealed a better lower to mid-level structure, with lower heights for a larger radius overall for RI systems. This suggests the RI core is physically

distinct from its surrounding environment. In general, for all RI definitions at all height levels, the highest heights are in the northeast quadrant quadrant of the composites, with low-levels for all RI definitions also exhibiting higher heights around the core, indicative of deeper convection (**Figure 6**). In the mid-levels and low-levels for 30kt/24-hours (four out of the six RI clusters) and 40kt/24-hours (two out of the five RI clusters) definitions, all of the RI clusters contain lower heights over the storm core for a larger radius. Map types for MSLP reveal instances when RI composites exhibit a smaller diameter of lower MSLP over the storm center (cluster 6 for RI using 30kt/24-hours and cluster 2 for 40kt/24-hours) with tighter gradients. Comparing these results to non-RI composites, three of the seven clusters maintain a uniform appearance (30kt/24-hours) or even mirror a traditional midlatitude trough/ridge pattern (in one non-RI map type). It is important to note that two non-RI cases using the 40kt/24-hours definition had larger regions of lower MSLP, which is explainable given the frequency of strong (category 3 or 4) non-RI storms associated with this RI definition (12% of the non-RI dataset). Regardless, the dominant pattern among all clusters shows a tighter gradient in low-level geopotential height and MSLP surrounding the TC core in RI systems. Permutation testing revealed a magnitude difference most apparent with MSLP composites for all RI definitions, where RI cases are exhibiting a statistically significantly larger radius of lower heights and pressures than for the non-RI systems, especially for 25kt and 30kt definitions. These results are supported by permutation test results for geopotential heights, which reveal the storm center in the low- and mid- levels as statistically significant at the 95% level in distinguishing between RI and non-RI storms (**Table 4**). It is also notable that the region of significance for MSLP increases as the wind definition increases. In other words, the 40kt/24-hours has the entire permutation map exhibiting statistical significance suggesting geopotential heights are more distinct; however, this could be an artifact of the 40kt definition containing category 4 and 5 storms making up 70% of the dataset versus non-RI containing at most category 4 (4%).

	T-mode analysis for geopotential height and MSLP					
	25kt/24-hours		**30kt/24-hours**		**40kt/24-hours**	
Variable	**Mag. difference (%)**	**Permutation significance (%)**	**Mag. difference (%)**	**Permutation significance (%)**	**Mag. difference (%)**	**Permutation significance (%)**
Geo. height 850 hPa	<5	11	<5	49	<5	**83**
Geo. height 700 hPa	<5	5.5	<5	19	<5	42
Geo. height 500 hPa	<5	13	<5	30	<5	12
Geo. height 200 hPa	<5	53	<5	**95**	<5	**96**
MSLP	<5	36	<5	**92**	<5	**100**

Percent significance values greater than 70 are bolded.

Table 4. T-mode analysis results for geopotential height and MSLP. Magnitude difference (%) for RI greater than non-RI composites and percent significance results from permutation tests for each variable examined for each RI definition.

Variable	T-mode analysis for thermodynamic variables					
	25kt/24-hours		30kt/24-hours		40kt/24-hours	
	Mag. difference (%)	Permutation significance (%)	Mag. difference (%)	Permutation significance (%)	Mag. difference (%)	Permutation significance (%)
Spec. humidity 850 hPa	<5	39	<5	**77**	8	**90**
Spec. humidity 700 hPa	6	33	10	69	12	67
Spec. humidity 500 hPa	14	33	13	55	18	38
Spec. humidity 300 hPa	27	40	21	51	22	44
Equiv.pot. temp. 850 hPa	<5	47	<5	**90**	<5	**93**
Equiv. pot. temp. 700 hPa	<5	50	<5	**90**	<5	**94**
Equiv. pot. temp. 500 hPa	<5	56	<5	**90**	<5	**95**
Equiv. pot. temp. 300 hPa	<5	**98**	<5	**100**	<5	**100**
Static stability 850 hPa	<5	2.4	<5	0.6	<5	19
Static stability 700 hPa	<5	16	<5	30	<5	82
Static stability 500 hPa	7.5	**79**	<5	**96**	6	**95**
Latent heat flux	16	58	14	35	11	29
CAPE	<5	46	<5	53	<5	62
CIN	<5	18	<5	5.5	<5	9.1
Skin temp	<5	70	<5	67	<5	60

Percent significance values greater than 70 are bolded.

Table 5. Same as **Table 4**, but for thermodynamic variables.

3.2.2. Thermodynamic characteristics

Specific humidity (25kt/24-hours and 30kt/24-hours) throughout the atmospheric profile contain larger magnitudes (see **Table 5**) for a greater diameter around the storm center and in the northeast quadrant quadrant for RI cases. RI TCs also contain maximum magnitude over the storm center in the mid- and upper- levels, or in the northeast quadrant quadrant, compared to non-RI cases which see a shift of the maximum magnitude towards the ENE region for 25kt/24-hours and 30kt/24-hours definition (**Figure 7**). Cross sections show drier air infiltrating through the inflow regions of the non-RI storm (west side of latitudinal cross section for 25kt/24-hours definition) compared to a more even distribution for RI clusters on either side of the storm center (**Figure 8**).

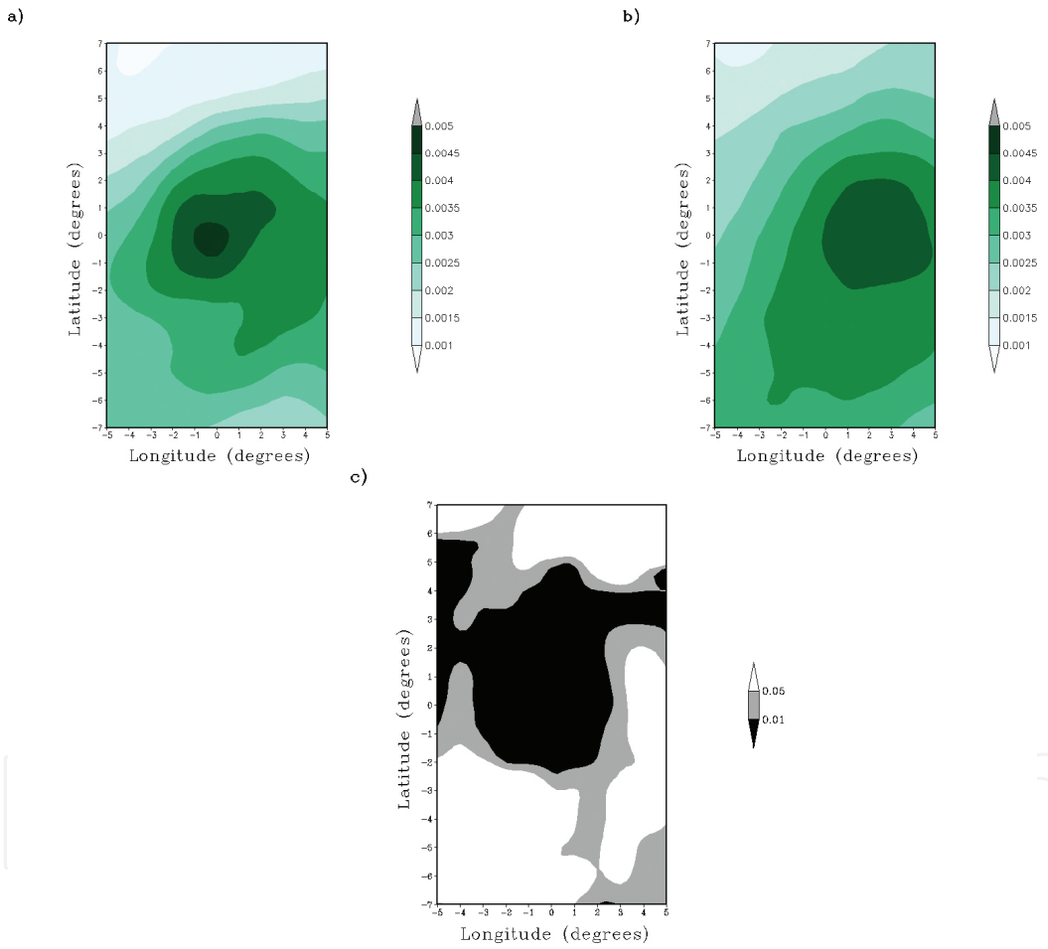

Figure 7. Specific humidity ($kgkg^{-1}$) composites at 500 hPa using 30kt/24-hours definition for cluster 5 RI (panel a) and cluster 6 non-RI (panel b). Permutation tests results (panel c–shaded areas are significant at α=0.05 or less) revealed the storm center as significant in discriminating between RI and non-RI events.

Equivalent potential temperature (θ_e) fields show similar magnitudes among RI and non-RI cases, although the radius of maximum θ_e is larger with the RI map type, suggesting the potential energy over the storm center is the important feature here. Additionally, the θ_e field is largely symmetric around the storm center for RI map types (**Figure 9a**). However, for the

non-RI using the 25kt/24-hours definition, the θ_e field is non-symmetric, instead showing a tilted core in the composite fields (**Figure 9b**). This tilt suggests a cutting off of the moisture source over the storm center, especially in the mid- and upper- levels. These results do not hold up as well for the 30kt/24-hours and 40kt/24-hours RI definitions, as there are non-RI composites which show symmetric latitudinal θ_e cross sections. While the more intense non-RI TCs have clustered together, distinguishing them from the non-RI group itself, it hinders classification ability using these RI definitions. Permutation tests revealed that at all pressure levels, for all RI definitions, the region directly over the storm center, as well as the inflow region for 25kt and 30kt definitions, is statistically significant at the 95% level in discriminating RI versus non-RI systems.

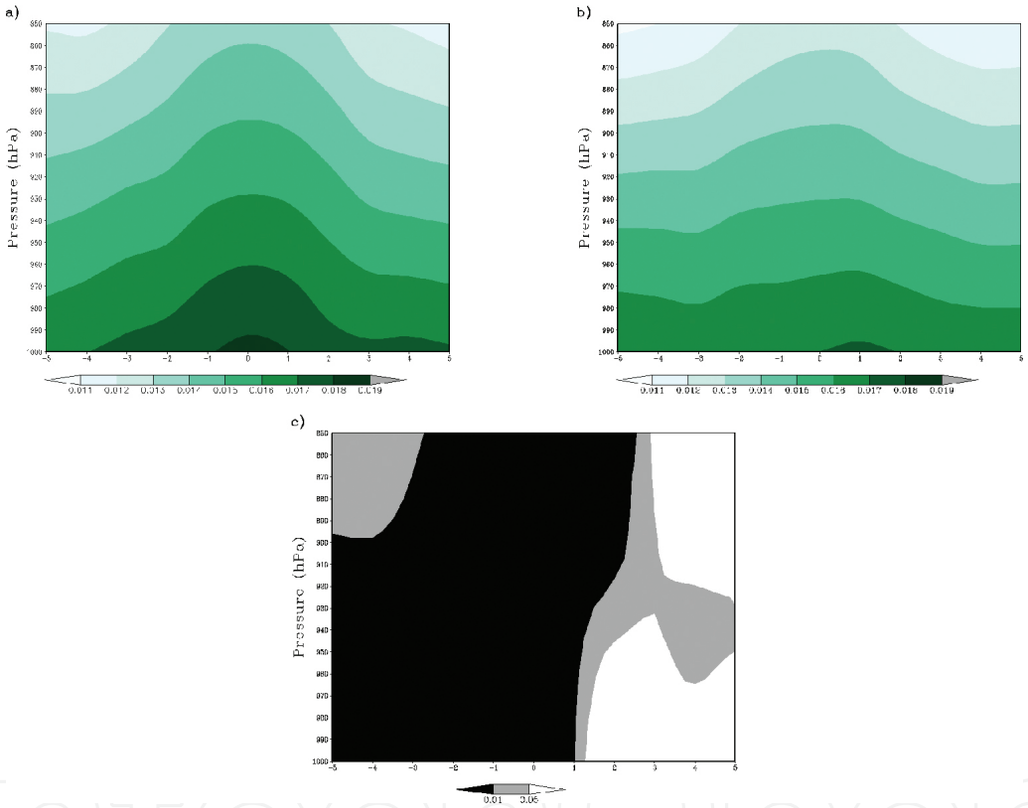

Figure 8. Latitudinal cross section for specific humidity (kgkg^{-1}) composites 1000–850 hPa using the 25kt/24-hours definition for cluster 5 RI (panel a) and cluster 3 non-RI (panel b). Permutation tests (panel c–shaded areas are significant at α=0.05 or less) revealed the storm center and inflow region as statistically significantly different.

Static stability at 500 hPa, on average revealed magnitudes were approximately the same for all definitions between RI and non-RI storms. However, RI clusters, which contained stronger TCs (i.e. category 4 and 5s), had a closed off maximum static stability center over the core of the storm for all RI definitions (**Figure 10**). Permutation tests confirm stability in the mid-levels as statistically significant in discriminating between RI and non-RI systems for nearly the entire storm domain. Notably, for the 40kt/24-hours definition, the storm center in the low-levels was also significant, but is likely a result of higher magnitudes (i.e. category 5 cases) for these RI events.

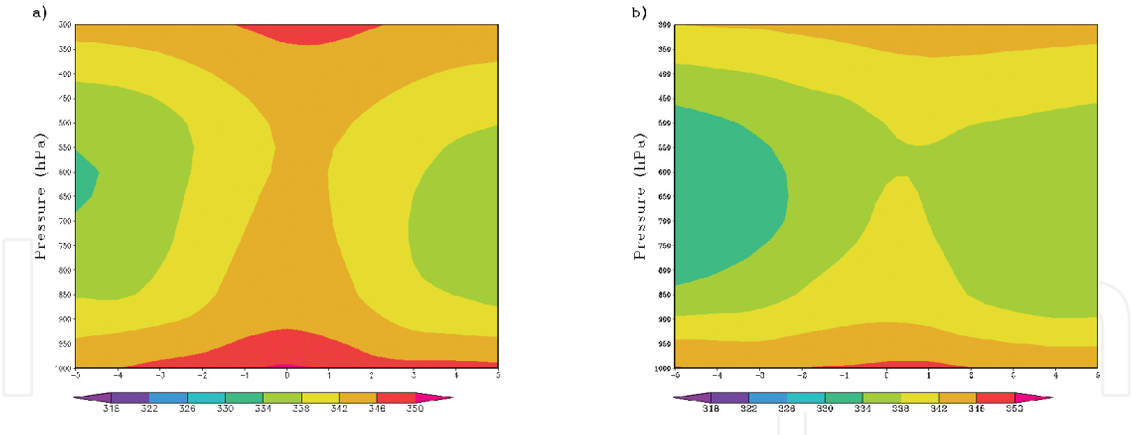

Figure 9. Latitudinal cross section composites for equivalent potential temperature (K) 1000–300 hPa using the 25kt/24-hours definition for cluster 5 RI (panel a) and cluster 3 non-RI (panel b).

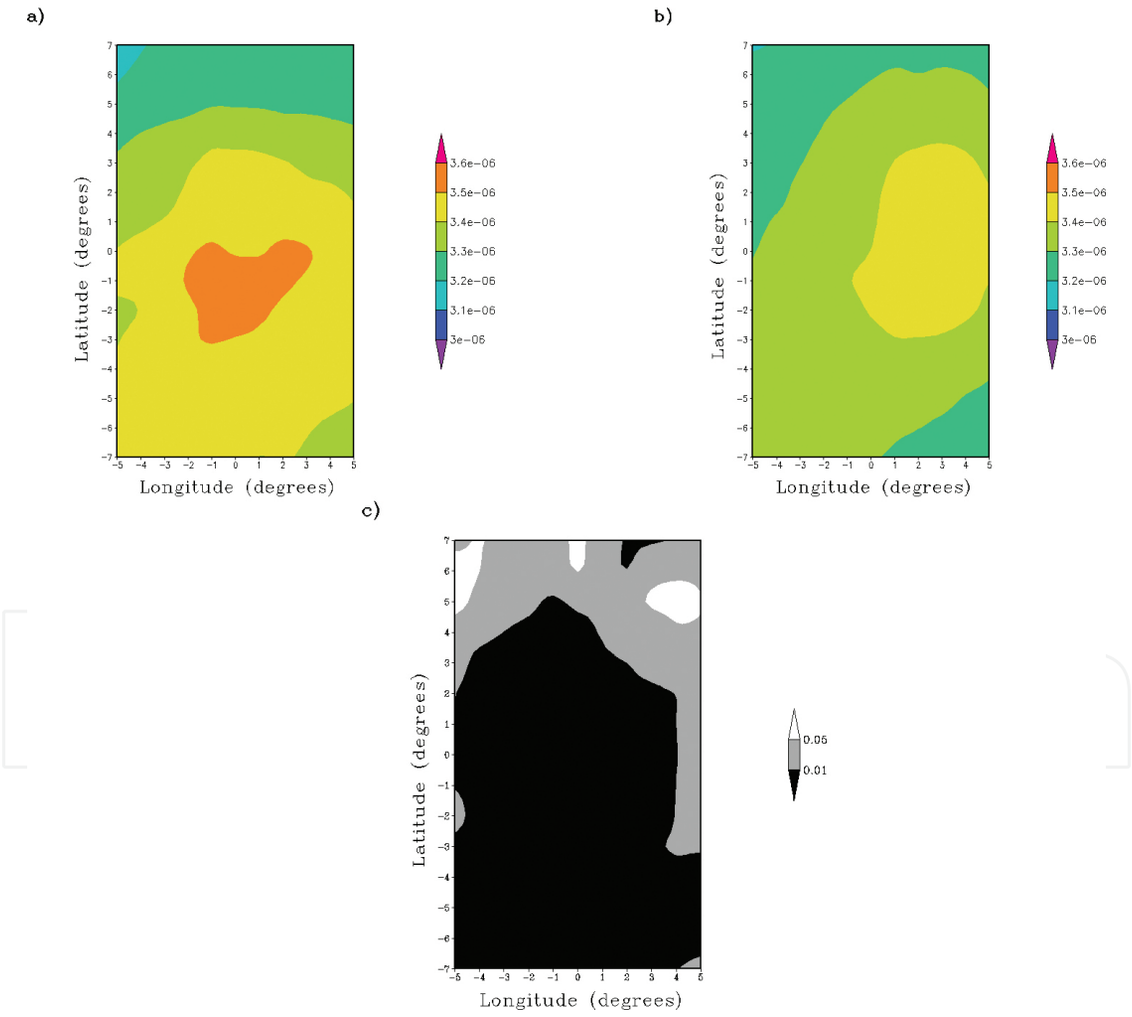

Figure 10. Static stability (K/Pa) composites at 500 hPa using 40kt/24-hours definition for cluster 2 RI (panel a) and cluster 3 non-RI (panel b). Permutation tests (panel c–shaded areas are significant at α=0.05 or less) revealed magnitude discrimination for nearly the entire storm domain.

http://dx.doi.org/10.5772/63988

3.2.3. Kinematic characteristics

The first kinematic field considered was upper-level (200 hPa) divergence. Divergence (25kt/24-hours and 30kt/24-hours) showed RI and non-RI clusters similar in both magnitude and region of greatest divergence in the northeast quadrant quadrant of the systems (**Figure 11**); however, the 40kt/24-hours definition revealed RI systems had 30% larger magnitude near the storm center and in the northeast quadrant quadrant. RI cases, for all definitions, tended to have a larger coverage area of the composite exhibiting divergence, despite the similarities in the spatial orientation of the divergence on the composite maps. Permutation tests supported the conclusion that divergence magnitude (**Table 6**), rather than spatial orientation, was the distinguishing characteristic between RI and non-RI storms at a 95% significance level.

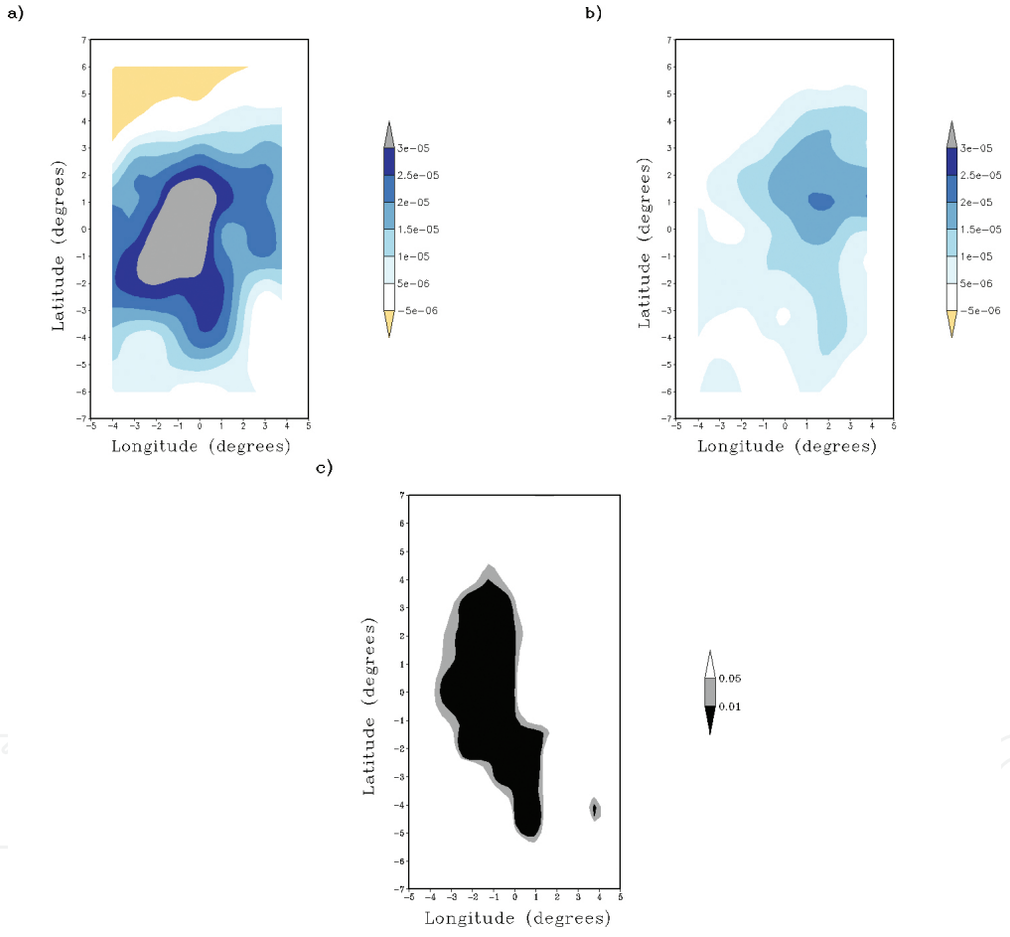

Figure 11. Divergence (s^{-1}) composites at 200 hPa using 30kt/24-hours definition shows an example of how cluster 5 RI (panel a) and cluster 6 non-RI (panel b) clusters are different in both magnitude and region of greatest divergence in the northeast quadrant quadrant of the systems. Permutation tests (panel c–shaded areas are significant at α=0.05 or less) revealed a region over the storm center as significant.

For relative vorticity, using both the 25kt/24-hours and 30kt/24-hours definitions, positive vorticity is noted in three out of the six RI clusters in proximity to storm center in the upper levels, which is notably absent from non-RI cluster map types. For the 40kt/24-hours definition,

three out of five RI map types exhibited this feature as well, while only two out of seven non-RI map types showed the same positive vorticity area (**Figure 12**). Vorticity magnitudes were larger for RI TCs with all map types (at all levels) and definitions, and also the vorticity gradient near the center was steeper within the RI system versus the non-RI. The only exception was at 700mb, in which vorticity features are similar in both RI and non-RI. Permutation tests show that over the storm center, for all three pressure levels, all RI definitions, had a 95% level of significance in distinguishing RI from non-RI cases. Notably, the area of statistical significance around the storm center is larger in the mid- levels.

	T-mode analysis for kinematic variables					
	25kt/24-hours		**30kt/24-hours**		**40kt/24-hours**	
Variable	**Mag. difference (%)**	**Permutation significance (%)**	**Mag. difference (%)**	**Permutation significance (%)**	**Mag. difference (%)**	**Permutation significance (%)**
Vorticity 700 hPa	17	12	35	11	28	16
Vorticity 500 hPa	40	19	22	15	38	19
Vorticity 200 hPa	100	22	100	17	28	14
Divergence 200 hPa	<5	23	<5	21	30	21
Directional shear 850–200 hPa	<5	12	<5	3.4	<5	8.5
Speed shear 850–200 hPa	47	**76**	30	**81**	33	**75**

Percent significance values greater than 70 are bolded.

Table 6. Same as **Table 4**, but for kinematic variables.

Map types of vertical speed shear (850–200 hPa – **Figure 13**), thought to be undesirable for RI to occur, revealed weaker 200 hPa winds than the 850 hPa winds within the RI. This is indicative of a closed off environment around the core for the RI systems to a greater degree than the non-RI. Permutation tests revealed all but the southwest quadrant to be statistically significant at the 95% level at discriminating RI from non-RI systems for all RI definitions.

3.2.4. Non-significant variables

CAPE, CIN, vertical velocity at 850 hPa, latent heat flux, sensible heat flux, static stability at 850- and 700-hPa, and skin temperature composites, while all examined, did not reveal

meaningful differences with regards to spatial orientation or magnitude for distinguishing between RI and non-RI cases. While some of the magnitudes were greater for RI clusters containing stronger systems (i.e. category 4 and 5 TCs), other non-RI clusters exhibited similar magnitudes which consisted mainly of tropical storm strength systems. Latent heat flux for example, revealed that for the 25kt/24-hour definition, more latent heat flux was available throughout the inflow region and around the core of the RI cases. However, with the 30kt/24-hour and 40kt/24-hour definitions, the main distinguishing feature seemed to only be higher magnitudes throughout the atmospheric profile. Otherwise, permutation tests surprisingly revealed the NW and northeast quadrant quadrant of the maps for all RI definitions as statistically significant at the 95% level for both CAPE and skin temperature. This is attributed to land influences of some TCs which were in proximity to land when the greatest intensification occurred. Results confirmed a lack of statistical significance in discriminating RI from non-RI with CIN, but confirmed a decent discrimination of magnitude with latent heat flux and sensible heat flux (**Table 5**). However, again, these results are likely being influenced by the proximity to land of some TCs, which would affect 1000 hPa level results for these variables.

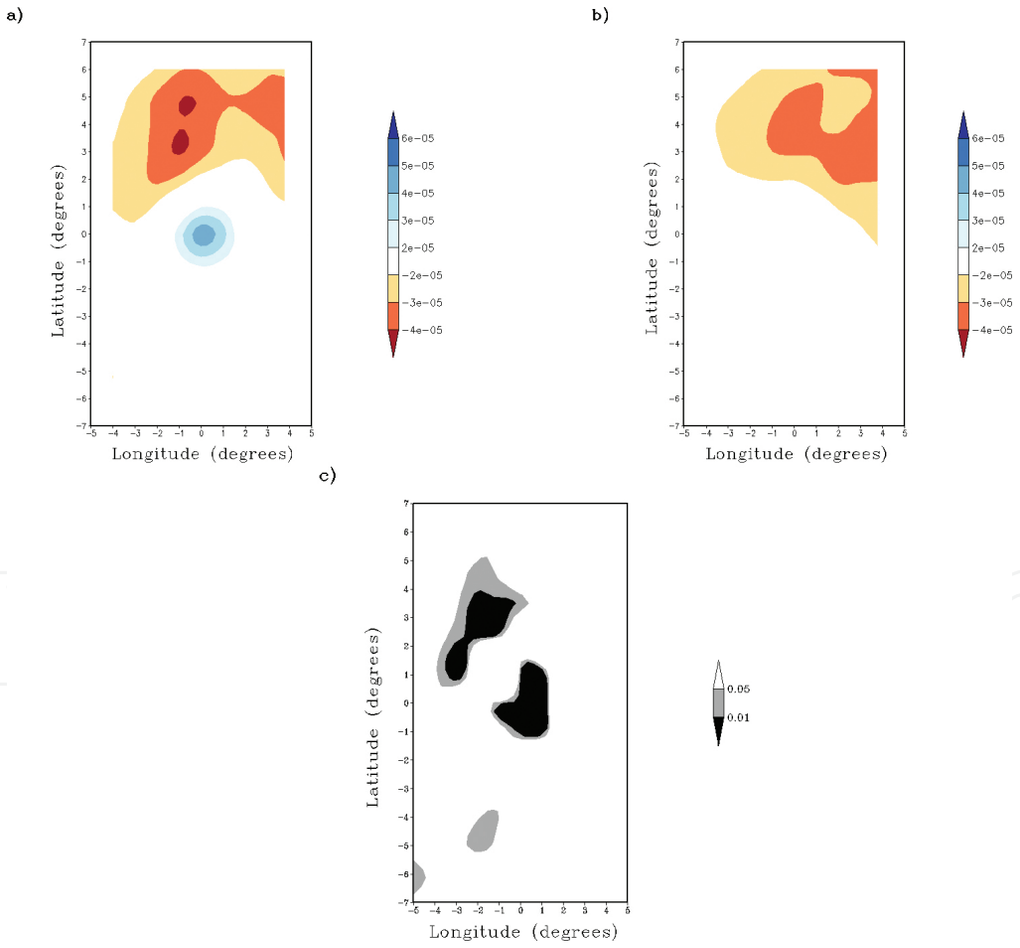

Figure 12. Relative vorticity (s^{-1}) composites at 200 hPa using 40kt/24-hours definition for cluster 2 RI (panel a) and cluster 3 non-RI (panel b). Permutation tests (panel c–shaded areas are significant at α=0.05 or less) revealed the area over the storm center to be statistically significant in distinguishing between the two event types.

Overall, the T-mode analysis revealed the discriminating spatial and magnitude differences between RI and non-RI storms. As suspected through S-mode analysis, moisture and surface temperature patterns, as well as variables indicating environmental influence including geopotential heights in the upper levels, relative vorticity, divergence, and static stability in the mid-levels had the largest influences on TC RI processes.

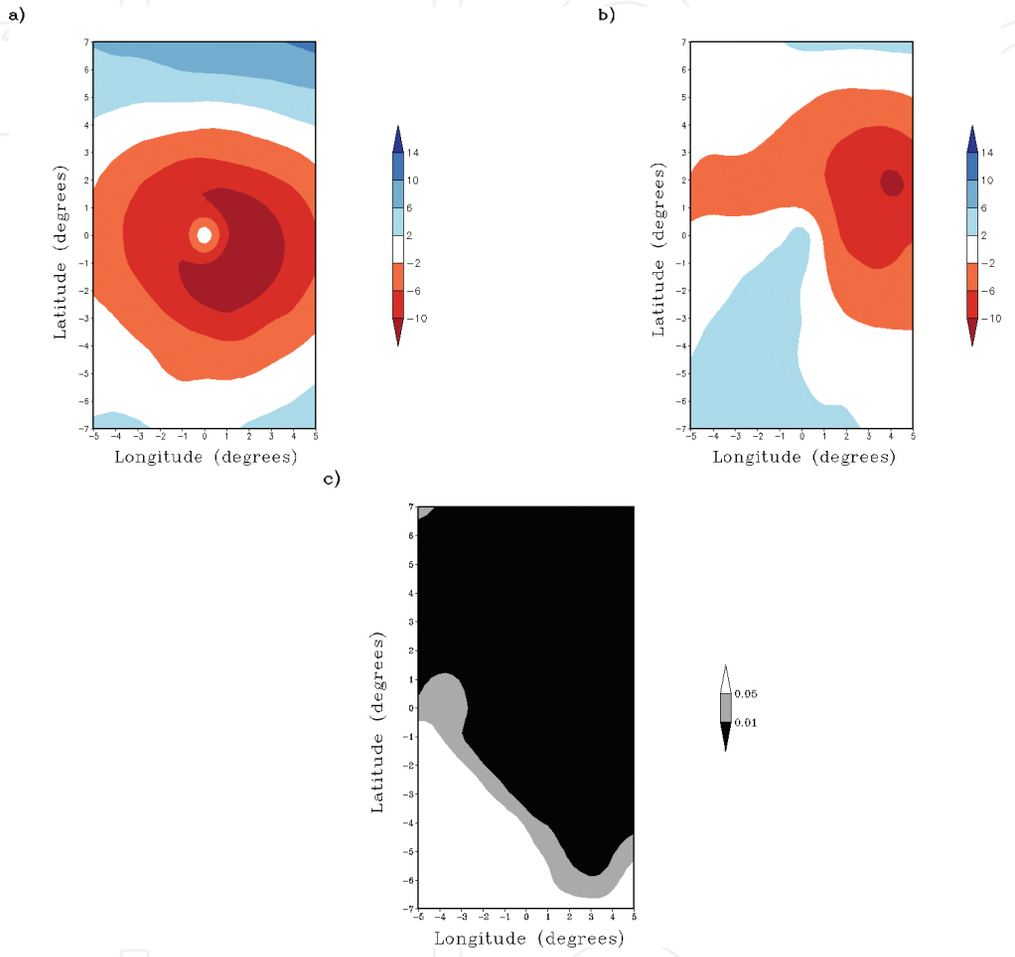

Figure 13. Vertical speed shear (ms^{-1}) composites at 850–200 hPa using 25kt/24-hours definition for cluster 5 RI (panel a) and cluster 3 non-RI (panel b). Permutation tests (panel c–shaded areas are significant at α=0.05 or less) revealed nearly the entire map as statistically significant.

4. Conclusion

Distinguishing meteorological characteristics of RI and non-RI storm structure is critically important in order to improve statistical model prediction of the onset of RI. This research made efforts to continue improvement in identifying relevant large-scale internal dynamics of TCs undergoing RI in the North Atlantic basin, specifically noting important diagnostic variables in three-dimensional space. Base-state, as well as composite derived, meteorological parameters were evaluated through both S-mode and T-mode RPCA for three RI definitions.

Specifically with T-mode, hierarchical cluster analysis techniques were used to formulate map types for RI and non-RI systems. To understand the internal dynamics within these complex systems, variables examined included: geopotential heights, temperature, u and v wind components, specific humidity, MSLP, CAPE, CIN, latent heat flux, sensible heat flux, surface temperature, vertical velocity at 850 hPa, divergence at 200 hPa, relative vorticity, vertical directional and speed shear, equivalent potential temperature, and static stability.

S-mode analysis results demonstrated the difficulty of establishing characteristic attributes for classifying RI and non-RI storms, as the base-state fields considered were equally present in RI and non-RI events for all RPCs. Two of the six RPC groups contained cases that were indicative of strong, well-structured TCs, exhibiting what you would expect for a sustainable environment for TC continuation and strengthening, regardless of storm type. Whereas, four of the six RPC groups contained cases influenced by baroclinic environmental effects on TCs, which further aids in the positive/negative aspects of environmental influence on TCs. While stronger outflow can lower stability, enhancing the outflow, it can also be detrimental to a TC [20, 21]. Despite this, results indicated a modest classification ability of RI and non-RI events through the temperature and moisture patterns, as well as those variables that would be more indicative of environmental interaction.

T-mode analysis, on the other hand, revealed several important distinguishing spatial features between RI and non-RI systems. Most notably:

- Geopotential heights and MSLP in the low- and mid- levels were statistically significantly different between RI and non-RI systems for all RI definitions, where RI systems maintained lower heights directly over the core and higher heights around the core and in the northeast quadrant quadrant for a larger radius. These results suggest deeper convection for RI systems, re-emphasizing the importance of convective processes around the core of a TC [2, 4, 22, 23].
- Specific humidity throughout the atmospheric profile contained larger magnitudes for a greater diameter around the storm center, as well as in the northeast quadrant quadrant for RI cases (which is in agreement with geopotential heights). Specifically, for the mid- and upper- levels, non-RI cases exhibited a shift of the largest specific humidity magnitudes towards the ENE region and cross sections suggested drier air infiltrating non-RI cases within the inflow regions of the storm for the 25kt/24-hours definition. This was in contrast to a more uniform horizontal and vertical moisture distribution in RI storms.
- Equivalent potential temperature for all RI definitions gave similar results to specific humidity, where the focus of the potential energy was over the storm center for RI cases. Non-RI cases instead exhibited a shift towards the east-northeast (creating the tilted appearance in the composites). This lack of symmetry in non-RI storms for the 25kt/24-hours definition, suggests a cutting off of the moisture and heat source over the storm center, especially in the upper-levels. This region over the storm center was significant in discriminating and indicates enhanced eyewall convection and TC intensity [23].
- Static stability for all RI definitions revealed RI systems were statistically significantly more stable over the storm center in the mid-levels than non-RI systems. This result implies a

resistance to upward vertical motion, forcing subsidence over the storm center [5, 20], but also resistance to adverse effects of the environment, such as vertical shear and Rossby penetration depth, preventing tilting of the TC and allowing for maintenance of the vertical thermal structure [24, 25].

- Divergence at 200 hPa (25kt/24-hours and 30kt/24-hours) showed RI and non-RI cluster composites similar in both spatial location and magnitude of greatest divergence in the northeast quadrant quadrant for the two types of systems. However, RI composites tended to have a statistically significantly larger magnitude.
- Relative vorticity at 200 hPa for the 25kt/24-hours and 30kt/24rs revealed three RI clusters contained an upper-level area of positive vorticity over the storm center. This feature only appeared for the 40kt/24-hours definition for non-RI systems (which is attributed to occurrence of category 4 TC events). Throughout the mid- and upper- levels, RI cases had significantly higher magnitudes over the storm center, indicating a stronger spin.
- Shear, often thought to hinder TC intensification by creating asymmetry in eyewall convection resulting in a loss of the warm core at upper levels through tilting [24–27], revealed vertical speed shear had a much larger area of statistical significance in discriminating RI from non-RI systems for all RI definitions, compared to vertical directional shear currently used in operational forecasts [1].
- CAPE and skin temperature did not reveal any distinguishing feature between RI and non-RI cases through composite analysis. However, permutation tests suggested the NW and northeast quadrant quadrant of the maps for all RI definitions as statistically significant at distinguishing between storm types for both. Latent heat flux, fundamental in the maintenance of convection and increasing kinetic energy [23, 28], showed that RI systems have higher magnitudes for a larger area over the core, for all RI definitions, and throughout the inflow region for the 25kt/24-hours and 30kt/24-hours definitions. However, land masses could be influencing results at the 1000 hPa pressure level for these three, and the other surface variables; therefore, distinguishing whether these fields are different among RIs and non-RIs remains unclear.

While results of the RPCA analysis confirm previous findings such as the importance of moisture supply, stability within the core, and stronger relative vorticity for RI systems, it also argues against research findings suggesting magnitude is the main distinguisher between RI and non-RI events [29]. Results presented suggest the symmetry of the equivalent potential temperature and specific humidity profiles throughout the atmospheric column, as well as the storm-centered placement of these variables, and stability, directly over the inner-core (instead of shifted to the east-northeast as with several non-RI composites given lower RI definitions) are significant in discrimination of these event types. While there were some shortcomings, such as proximity to land potentially influencing results in the low levels and the inability to fully resolve the inner-core due to model resolution, the results provide a framework of diagnosis for RI processes within TCs. This framework, combined with an improved statistical modelling scheme, will ideally be of use for improving TC intensity forecasts in operational meteorology.

Acknowledgements

This work was funded through the Northern Gulf Institute by NOAA Grant #NA11OAR4320199 at Mississippi State University.

Author details

Alexandria Grimes and Andrew E. Mercer*

*Address all correspondence to: a.mercer@msstate.edu

Northern Gulf Institute, Mississippi State University, Mississippi State, MS, USA

References

[1] Kaplan J, Rozoff CM, DeMaria M, Sampson CR, Kossin JP, Velden CS, Cione JJ, Dunion JP, Knaff JA, Zhang JA, Dostalek JF. Evaluating environmental impacts on tropical cyclone rapid intensification predictability utilizing statistical models. Weather and Forecasting. 2015 Oct;30(5):1374-96.

[2] Kaplan J, DeMaria M. Large-scale characteristics of rapidly intensifying tropical cyclones in the North Atlantic basin. Weather and Forecasting. 2003 Dec;18(6):1093-108.

[3] Hendricks EA, Peng MS, Fu B, Li T. Quantifying environmental control on tropical cyclone intensity change. Monthly Weather Review. 2010 Aug;138(8):3243-71.

[4] Rozoff CM, Velden CS, Kaplan J, Kossin JP, Wimmers AJ. Improvements in the probabilistic prediction of tropical cyclone rapid intensification with passive microwave observations. Weather and Forecasting. 2015 Aug;30(4):1016-38.

[5] Vigh JL, Schubert WH. Rapid development of the tropical cyclone warm core. Journal of the Atmospheric Sciences. 2009 Nov;66(11):3335-50.

[6] Sitkowski M, Barnes GM. Low-level thermodynamic, kinematic, and reflectivity fields of Hurricane Guillermo (1997) during rapid intensification. Monthly Weather Review. 2009 Feb;137(2):645-63.

[7] Rozoff CM, Kossin JP. New probabilistic forecast models for the prediction of tropical cyclone rapid intensification. Weather and Forecasting. 2011 Oct;26(5):677-89.

[8] Kaplan J, DeMaria M, Knaff JA. A revised tropical cyclone rapid intensification index for the Atlantic and eastern North Pacific basins. Weather and forecasting. 2010 Feb; 25(1):220-41.

[9] Jarvinen BR, Neuman CJ, Davis MA. A tropical cyclone data tape for the North Atlantic basin. NOAA Tech. Memo. NWS NHC-22. 1988. Mar: 24 pp.

[10] Hamill TM, Bates GT, Whitaker JS, Murray DR, Fiorino M, Galarneau Jr TJ, Zhu Y, Lapenta W. NOAA's second-generation global medium-range ensemble reforecast dataset. Bulletin of the American Meteorological Society. 2013 Oct;94(10):1553-65.

[11] Mercer AE, Shafer CM, Doswell III CA, Leslie LM, Richman MB. Synoptic composites of tornadic and nontornadic outbreaks. Monthly Weather Review. 2012 Aug;140(8): 2590-608.

[12] Grimes A, Mercer AE. Synoptic-scale precursors to tropical cyclone rapid intensification in the Atlantic Basin. Advances in Meteorology. 2015 May 27; 2015: 16pp.

[13] Michael B R, Andrew E M, Lance M L, Charles A III D, Chad M S. High dimensional dataset compression using principal components. Open Journal of Statistics. 2013 Oct 9;2013.

[14] Richman MB. Rotation of principal components. Journal of climatology. 1986 Jan 1;6(3): 293-335.

[15] Richman MB, Lamb PJ. Climatic pattern analysis of three-and seven-day summer rainfall in the central United States: some methodological considerations and a regionalization. Journal of Climate and Applied Meteorology. 1985 Dec;24(12):1325-43.

[16] Wilks DS. Statistical Methods in the Atmospheric Sciences. Oxford: Academic press; 2011.

[17] Rousseeuw PJ. Silhouettes: a graphical aid to the interpretation and validation of cluster analysis. Journal of computational and applied mathematics. 1987 Nov 1;20:53-65.

[18] Markowski P, Richardson Y. On the classification of vertical wind shear as directional shear versus speed shear. Weather and Forecasting. 2006 Apr;21(2):242-7.

[19] Bluestein, H. Synoptic Dynamic Meteorology in Midlatitudes: Principles of Kinematics and Dynamics, Vol. 1. 1st ed. New York, NY: Oxford University Press; 1992. 430 p.

[20] Holland G, Merrill RT. On the dynamics of tropical cyclone structural changes. Quarterly Journal of the Royal Meteorological Society. 1984 Jul 1;110(465):723-45.

[21] Molinari J, Vollaro D. External influences on hurricane intensity. Part I: outflow layer eddy angular momentum fluxes. Journal of the Atmospheric Sciences. 1989 Apr;46(8): 1093-105.

[22] Rogers R. Convective-scale structure and evolution during a high-resolution simulation of tropical cyclone rapid intensification. Journal of the Atmospheric Sciences. 2010 Jan;67(1):44-70.

[23] Li Q, Wang Y, Duan Y. Impacts of evaporation of rainwater on tropical cyclone structure and intensity—a revisit. Journal of the Atmospheric Sciences. 2015 Apr;72(4):1323-45.

[24] DeMaria M. The effect of vertical shear on tropical cyclone intensity change. Journal of the Atmospheric Sciences. 1996 Jul;53(14):2076-88.

[25] Jones SC. The evolution of vortices in vertical shear. I: initially barotropic vortices. Quarterly Journal of the Royal Meteorological Society. 1995 Apr 1;121(524):821-51.

[26] Wang Y, Holland GJ. Tropical cyclone motion and evolution in vertical shear. Journal of the Atmospheric Sciences. 1996 Nov;53(22):3313-32.

[27] Frank WM, Ritchie EA. Effects of vertical wind shear on the intensity and structure of numerically simulated hurricanes. Monthly Weather Review. 2001 Sep;129(9):2249-69.

[28] Ma Z, Fei J, Huang X, Cheng X. Contributions of surface sensible heat fluxes to tropical cyclone. Part I: evolution of tropical cyclone intensity and structure. Journal of the Atmospheric Sciences. 2015 Jan;72(1):120-40.

[29] Kowch R, Emanuel K. Are special processes at work in the rapid intensification of tropical cyclones?. Monthly Weather Review. 2015 Mar;143(3):878-82.

IntechOpen